Molecular dynamics simulations

2004 J. Phys.: Condens. Matter 16 S429

(http://iopscience.iop.org/0953-8984/16/5/006)

INSTITUTE OF PHYSICS PUBLISHING JOURNAL OF PHYSICS: CONDENSED MATTER

J. Phys.: Condens. Matter **16** (2004) S429–S453 PII: S0953-8984(04)57979-1

Molecular dynamics simulations

Kurt Binder[1], Jürgen Horbach[1], Walter Kob[2], Wolfgang Paul[1] and Fathollah Varnik[3]

[1] Institut für Physik, Johannes Gutenberg-Universität, D-55099 Mainz, Staudinger Weg 7, Germany
[2] Laboratoire des Verres, Université Montpellier II, F-34094 Montpellier, France
[3] Centre de Calcul Atomique et Moleculaire (CECAM), ENS-Lyon, 46, Allée d'Italie, F-69007 Lyon, France

Received 8 January 2003
Published 23 January 2004
Online at stacks.iop.org/JPhysCM/16/S429 (DOI: 10.1088/0953-8984/16/5/006)

Abstract

A tutorial introduction to the technique of molecular dynamics (MD) is given, and some characteristic examples of applications are described. The purpose and scope of these simulations and the relation to other simulation methods is discussed, and the basic MD algorithms are described. The sampling of intensive variables (temperature T, pressure p) in runs carried out in the microcanonical (NVE) ensemble (N = particle number, V = volume, E = energy) is discussed, as well as the realization of other ensembles (e.g. the NVT ensemble). For a typical application example, molten SiO_2, the estimation of various transport coefficients (self-diffusion constants, viscosity, thermal conductivity) is discussed. As an example of non-equilibrium molecular dynamics, a study of a glass-forming polymer melt under shear is mentioned.

(Some figures in this article are in colour only in the electronic version)

1. Introduction: scope and purpose of molecular dynamics simulations

1.1. Molecular dynamics and its relation to other methods of computer simulation

Computer simulations in condensed matter physics aim to calculate structure and dynamics from atomistic input [1–4]. The theoretical basis of this approach is statistical thermodynamics. The conceptually simplest approach is the classical molecular dynamics (MD) method [5–7]: one simply solves numerically Newton's equations of motion for the interacting many-particle system (atoms or molecules interacting, e.g., with pair potentials). The basics of the method therefore is nothing but classical mechanics, and one creates a deterministic trajectory in the phase space of the system. Now the idea is to simply take time averages of the observables of interest along this trajectory, and rely on the ergodicity hypothesis of statistical mechanics, which asserts that these time averages are equivalent to ensemble averages of the appropriate microcanonical (NVE) ensemble. Of course, Newton's equations of motion conserve the total

energy E, and hence the conjugate intensive thermodynamic variables such as temperature T and pressure p can only be inferred indirectly and exhibit fluctuations (since the particle number N is finite and sometimes even fairly small, such fluctuations must not be neglected and need careful consideration). Sometimes it is advantageous to directly realize other ensembles of statistical mechanics, such as the constant volume V–constant temperature T (NVT) ensemble or the NpT ensemble, and—as we shall see later—this is indeed feasible by introducing a coupling to appropriate 'thermostats' or 'barostats'.

An alternative way of carrying out an MD simulation at constant temperature is possible by introducing an artificial weak friction force, together with random forces whose strengths are controlled by the fluctuation–dissipation theorem. Such techniques are very common e.g. for the simulation of polymer melts [8, 9]. This method is very closely related in spirit to stochastic simulation methods such as 'Brownian dynamics' where one simulates a Langevin equation (the inertial term in the equation of motion being omitted). While dynamical correlations for such methods differ somewhat from strictly microcanonical MD methods, for the computation of static properties from averages along the stochastic trajectory in phase space such methods can be advantageous.

This statement is also true for the importance sampling Monte Carlo (MC) method [10, 11]. As is well known [4, 11], MC sampling means that one creates a random-walk-like trajectory in configuration space, controlled by transition probabilities that ensure the approach to thermal equilibrium via a detailed balance condition. Many of the practical aspects of computer simulations, such as 'statistical errors' and systematic errors due to the finite size of the simulated system or the finite 'length' of the simulated trajectory (or observation time, respectively), are shared by all these simulation methods.

However, one important caveat needs to be made: it is quantum mechanics that describes the basic physics of condensed matter, and not classical mechanics. However, attempting a numerical solution of the Schrödinger equation for a system of many nuclei and electrons is still premature and not at all feasible even on the fastest computers. Thus, one has to resort to approximations. One very popular approach is the '*ab initio* MD' or 'Car–Parrinello method' [12], where one includes some electronic degrees of freedom in MD via density functional theory (DFT) [13]. The huge advantage of this technique is that one no longer relies on effective interatomic potentials, which often are only phenomenologically chosen *ad hoc* assumptions, lacking any firm quantum chemical foundation. However, the disadvantage of this technique is that it is several orders of magnitude slower than classical MD, and hence only very short timescales and very small systems are accessible. Furthermore, the method is unsuitable to treat systems with van der Waals-like forces, such as in rare gases, where one is still better off with the simple Lennard-Jones (LJ) potential (perhaps amended by three-body forces) [1]. Also, normally ionic degrees of freedom are still treated classically. Alternatively, one can still use effective potentials between ions and/or neutral atoms as in classical MD or MC, but rely on quantum statistical mechanics for the ionic degrees of freedom: this is achieved by path integral Monte Carlo (PIMC) [14, 15] or path integral molecular dynamics (PIMD) [16–18]. Such techniques are indeed crucial for a study of solids at low temperatures, to ensure that their thermal properties are compatible with the third law of thermodynamics. For most fluids (of course, quantum liquids such as ^{3}He and ^{4}He are an exception) classical MD is fine, and will henceforth be considered exclusively in this article.

What information do we then desire to extract from the simulations? When we consider systems in thermal equilibrium, the first task is to calculate static properties. For example, in a fluid a basic property is the static structure factor $S(k)$ [19]

$$S(k) = \langle |\delta\rho(\vec{k})|^2 \rangle, \tag{1}$$

where $\delta\rho(\vec{k})$ is a spatial Fourier transform of density fluctuations, $\vec{k}$ being the wavevector. In addition, one wants to calculate time-dependent correlation functions, that describe the decay of small thermal fluctuations with time. A quantity of this type that will be discussed later is the intermediate scattering function $S(k, t)$,

$$S(k, t) = \langle \delta\rho(-\vec{k}, 0)\delta\rho(\vec{k}, t)\rangle. \tag{2}$$

If one considers systems out of thermal equilibrium, an important application of MD is the study of systems exhibiting a steady state flow under shear deformation. The purpose of such non-equilibrium molecular dynamics (NEMD) [20, 21] work can be the estimation of transport coefficients (e.g. the shear viscosity) if the deformation is weak enough that the system is still in the regime of linear response [19]. However, the study of nonlinear phenomena (such as 'shear thinning', a decrease of the effective viscosity with increasing shear rate [20, 21]) is also of interest [22]. In addition, one can also study non-steady-state transient behaviour, as occurs e.g. after a sudden quench from one state to another, where one wishes to study the approach of the system to its new thermal equilibrium. Classical examples of this problem are nucleation of fluid droplets in a supersaturated gas or the kinetics of phase separation in a binary mixture ('spinodal decomposition' [23]). However, often such processes are too slow, and cannot really be studied by NEMD, and instead one has to use simulations of coarse-grained models by non-equilibrium Monte Carlo (NEMC) [2, 4, 9, 11].

Now this list of simulation techniques and problems that one may simulate sounds wonderful—everything can be studied with computer simulation methods, even problems outside the standard realm of physics: the spontaneous formation of traffic jams on major roads [24], anomalous time-dependent autocorrelation functions of heart beats of human beings suffering from heart diseases [25], critical fluctuations at the stock market before a crash [26], shock waves that can destroy a silo used in agriculture when the grains of corn stored in it flow out at the wrong speed [27] etc. All these problems are in fact simulated by theoretical physicists using techniques very similar to MD or MC. However, one must nevertheless always keep in mind that computer simulations—as do all other techniques!—suffer from some very important technical limitations that the practitioner always must be aware of, just as an experimentalist in an inelastic scattering experiment must be aware of that the resolution of his energy and momentum transfer measurements limits his data analysis, and that in addition there are statistical errors due to limited intensity of the radiation source.

1.2. Limitations of computer simulations: when to choose which method?

The main limitation of atomistic simulations comes from the fact that one must often bridge many decades in spatial scale and even more decades in timescale to describe the phenomena of interest [28, 29]. As an example, we discuss here the problem of phase separation of a mixture of a polymer (such as polybutadiene) and its deuterated counterpart [30]. If one carries out a quenching experiment, suddenly reducing the temperature from a high value in the one phase region to a lower value inside the miscibility gap, and records the equal-time structure factor $S(k)$, equation (1), at different times t after the quench, one observes the growth of a peak at a position $k_m(t)$ [30]. Now polybutadiene is a flexible linear macromolecule, which in the molten state forms random-walk-like coils that exhibit nontrivial structure from the scale of covalent C–C and C–H bonds (i.e., of the order of 1 Å) to the coil radius (which is of the order of 10^2 Å, for the molecular weights used in the experiment). The collective length scale $\ell(t) \approx 2\pi/k_m(t)$ is already of the order of 1000 Å in the initial stage of phase separation, however. Clearly, such a study of cooperative phenomena of a large number of chains would be prohibitively difficult, if we tried a chemically realistic, atomistically detailed

description. Moreover, the description of effective potentials driving this phase separation between protonated and deuterated polymers which otherwise are chemically identical is quite subtle: in the framework of classical statistical mechanics, the masses of the particles cancel out from all static averages, and hence such a mixture would be an ideal mixture, perfectly miscible; no phase separation would ever occur. The reason that phase separation is observed in the experiment [30] is a quantum effect; the zero-point vibrational motions of hydrogens and deuterons differ: the lighter hydrogens need more space and this causes an effective repulsive interaction between unlike species.

An even greater problem is the disparity of timescales encountered in this example: while the timescale of bond length and bond angle vibrations is of the order of 10^{-13} s, already the time needed for a coil to renew its configuration can be estimated as 10^{-5} s, eight orders of magnitude larger than the vibration times, for the considered molecular weight [30] and temperature of the experiment. The collective dynamics, however, is even much slower, because the thermodynamic driving forces are very weak. Thus, the experiment shows [30] that the interesting phenomena happen on the timescales from a few seconds to 1000 s, when a scattering peak develops at $k_m(t)$ and first grows more or less at the same position and then shifts to smaller and smaller wavevectors as the coarsening of the structure proceeds. Moreover, while for the case of phase separation in metallic alloys the situation is better with respect to the length scale $k_m(t)$ [23, 31], $k_m(t) \sim 0.01$–0.1 Å^{-1}, the typical timescale is still from 0.1 to 10^3 s, and hence for a chemically realistic MD simulation, with a time step δt in the range from 1 to 10 fs, the task is quite hopeless; one would have to simulate over a range of 10^{15} time steps which is many orders of magnitude more than what is feasible nowadays.

Such slow phenomena as spinodal decomposition in solid metallic alloys or fluid polymer mixtures can only be simulated by very simplified coarse-grained models, where chemical detail is sacrificed, and one applies NEMC methods rather than MD. These coarse-grained simulations are nevertheless very useful, both for solid alloys [32] and for polymers [33]. In the latter case, several successive chemical monomers along the chain are integrated into one 'effective bond'. Moreover, one also simulates relatively short (unentangled) chains, and hence one does not attempt to study chains of large molecular weight as done in the experiment [30]. Even with these simplifications, it is difficult to deal with such long-wavelength phenomena: the computer simulation can never deal directly with the system in the thermodynamic limit; one can always only treat a finite system. In this case of spinodal decomposition of binary polymer mixtures [33] a cubic box containing a few hundred or a few thousand short polymer chains is studied. To avoid surface effects at the boundaries of the simulation box, periodic boundary conditions are used. Such systems are sometimes called quasi-infinite, but this is not quite true: the finite size of the system still has notable effects, e.g. the reciprocal space is 'quantized', since the only wavevectors that are compatible with the periodic boundary conditions are of the form

$$\vec{k} = (k_x, k_y, k_z) = \frac{2\pi}{L}(n_x, n_y, n_z), \tag{3}$$

where L is the size of the box and n_x, n_y, n_z are integers.

In practice one does find for this problem that the position $k_m(t)$ where the peak grows occurs near values of k where $\mu < 10$, and hence the discreteness of $\vec{k}$-space is a real practical problem. Despite such problems, the simulations of collective phenomena [32, 33] are useful, but it is always advisable to carefully pay attention to possible artifacts caused by the finite size of the simulation box.

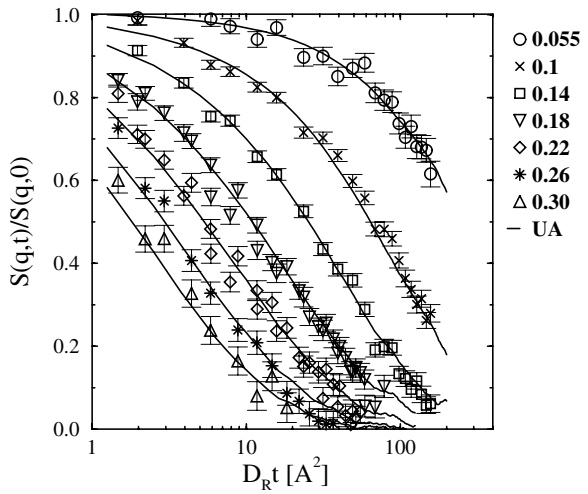

Figure 1. Intermediate dynamic structure factor versus scaled time as obtained from a neutron spin echo experiment (symbols) and computer simulation results (full curves). The time axis is scaled by the respective centre of mass diffusion coefficients D_R. The ordinate axis is scaled by the static (equal-time) single-chain structure factor $S(q, 0)$. The different symbols represent the different values of q, in units of Å^{-1}, as explained in the legend (from [35]).

1.3. Internal dynamics of polymer chains: an example of what can be done when models are carefully chosen

This example of unmixing in polymer blends [33] is not meant to imply that MD simulations for polymers are not feasible at all: on the contrary, MD work for polymers can be very useful and can even be compared to experiment quantitatively, but only for carefully selected problems! This is shown in an example [34, 35] dealing with the relaxation of the configuration of polymer coils. While for entangled chains with a degree of polymerization of the order of 10^3 the relaxation time τ_R of the coil configuration is typically at least 10^{-5} s, the choice of shorter non-entangled chains such as $C_{100}H_{202}$ brings τ_R down to about $\tau_R \approx 1$ ns, if a sufficiently high temperature is chosen ($T = 509$ K in this case). Figure 1 shows a comparison of data for the single-chain (normalized) coherent intermediate scattering function

$$S(q,t) = \frac{1}{N_p} \sum_{n,m=1}^{N_p} \langle \exp[\mathrm{i}\vec{q} \cdot (\vec{r}_n(t+t_0) - \vec{r}_m(t_0)] \rangle \tag{4}$$

obtained by the neutron spin echo technique, with MD simulation results of a suitable model. In equation (4), $\vec{q}$ is the scattering vector, N_p is the degree of polymerization of the chain ($N_p = 100$ here) and $\vec{r}_m(t_0)$ is the position of the mth monomer of a chain ($1 \leqslant m \leqslant N_p$) at time t_0. The average $\langle \cdots \rangle$ in the simulation is taken over all chains in the system and is also meant to represent the time average over the time t_0. Note that we have already made use of the fact that in thermal equilibrium a time-displaced correlation function as written on the rhs of equation (4) depends only on the difference t between the two times $t + t_0$ and t_0, and not on these two times separately.

It is seen from figure 1 that there is an almost perfect agreement between the experimental data and the simulations, over two decades in time and almost a decade in the wavevector, and in this scaled plot there is no adjustable parameter whatsoever! Thus, this agreement is by no means a trivial fitting exercise, but rather it is truly significant. While the original conclusion

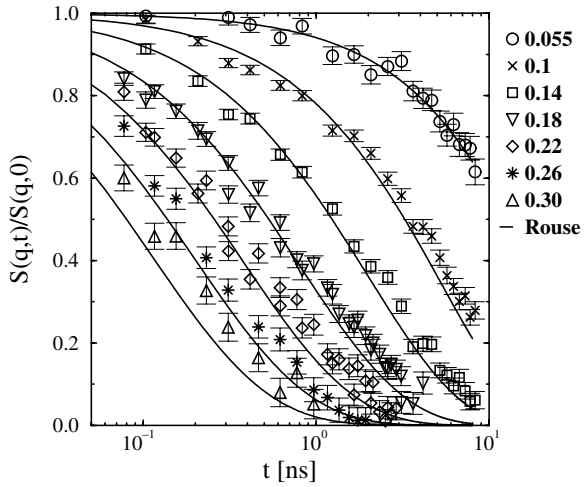

Figure 2. Normalized coherent intermediate scattering function for $C_{100}H_{202}$ plotted versus time, for the wavelength q (in Å^{-1}) as indicated in the legend. The full curves are the Rouse model prediction; the symbols denote the simulation results (from [35]).

of the experimentalists was that their data prove the validity of the Rouse model [36, 37], one now knows, thanks to the simulation (figure 2), that this is not quite correct. Remember that the Rouse model describes the polymer as a harmonic chain, which experiences friction and stochastic forces which represent the interactions with the surrounding chains. This simplistic model contains only two parameters, an effective size σ of a bead, and the friction coefficient ζ. Both are known from independent estimates of other quantities in the simulation (static structure factor $S(q, 0)$ and self-diffusion constant D_R of the chains, respectively). So again one can perform a comparison between the simulation and the theory without any adjustable parameters whatsoever (figure 2). One sees that the Rouse model works very well for small values of q, while it fails for larger wavelengths. Later experimental work did indeed confirm the conclusion of the simulations [35] that the Rouse model is not so perfect as originally claimed.

This figure also shows that $S(q, t)$ for typical values of q really does decay to zero on the scale of 1–10 ns. We emphasize again that this was only possible due to carefully chosen simulation parameters: $C_{100}H_{202}$ is a relatively short chain, and $T = 509$ K is a relatively high temperature. The experiment was deliberately done for such parameters to allow a meaningful comparison with a simulation. As was said above, for other parameters it could easily happen that the relaxation time for $q \approx R_g^{-1}$ (R_g being the gyration radius of the chains) is larger by a factor of 10^3–10^6 than in the present case. While at large enough q it still may be possible to study the relaxation in the 'time window' accessible for the scattering experiment, it would not make sense to compare with a computer simulation: the latter cannot reach thermal equilibrium if the Rouse time (the time needed to equilibrate the configuration of the *whole* chain) is so large. Note that it is often thought that there is always a direct correspondence between quantities that one can study by inelastic neutron scattering and the corresponding MD observations, since both methods have a 'time window' of about 1 ns. However, in an experiment one can invest a time of days or even weeks to carefully anneal the sample and thus prepare very good equilibrium. But this is not the case in a simulation: in MD work one almost always has to start from some initial state which is not yet characteristic for the desired equilibrium,

and let the system relax towards equilibrium with an MD run that can also last only a few nanoseconds! Therefore meaningful inelastic scattering experiments can study the relaxation of fast degrees of freedom in fluids rather close to the glass transition temperature of polymers or other glass-forming systems, since the system is in good thermal equilibrium. In contrast to this MD simulations of a corresponding model can reach equilibrium only at much higher temperatures, however. These simple considerations are almost obvious but nevertheless often ignored—therefore we emphasize these points here.

A related misconception is that an MD simulation is better when more chemical detail is included in the model: however, this attitude is completely wrong! In fact, the level of detail in the simulations of Paul *et al* [34, 35] normally neither included fluctuations in the lengths of the C–C bonds along the chain backbone, nor were the hydrogen atoms explicitly included: the bond length was kept at the experimental value $\ell_{cc} = 1.53$ Å, and the CH_2 groups were treated as 'united atoms' (also no full distinction between the CH_3 groups at the chain ends and the CH_2 groups in the interior was made). If one includes the hydrogens explicitly, the program is about a factor of ten slower, and a modest gain in accuracy of the model is more than outweighed by about three times larger statistical errors. Note that this dramatic slowing down of the code is inevitable due to the very stiff potentials that need to be included in such an 'all-atom' calculation and which necessitate then a particularly small time step (and also the number of atoms is three times larger). The potentials actually used for the simulations shown in figures 1 and 2 are bond angle potentials $U(\Theta)$ and torsion potentials $U(\phi)$ of the form

$$U(\Theta) = \tfrac{1}{2}k_\Theta(\cos\Theta - \cos\Theta_0)^2, \qquad U(\phi) = \sum_{n=0}^{5} a_n \cos^n(\phi), \tag{5}$$

while non-bonded monomers interact with an LJ potential

$$U(r_{ij}) = 4\varepsilon_{\alpha\beta}[(\sigma/r_{ij})^{12} - (\sigma/r_{ij})^6], \qquad \alpha, \beta \in \{CH_2, CH_3\}. \tag{6}$$

The parameters k_Θ, Θ_0, a_n, $\varepsilon_{\alpha\beta}$ and σ are given in [34, 35]. In principle, such effective potentials for classical MD simulations should be deduced from quantum chemical calculations. However, polyethylene is a much too large molecule to do that: only the bond angle and torsional potentials have a quantum chemical basis, although even on this issue there is no full consensus between different groups. Of course, it is clear that the LJ potential used here (equation (6)) is completely *ad hoc*, and the parameters are just optimized in order to fit as many experimental data as possible. For the case of $C_{100}H_{202}$, a box of linear dimension $L = 50$ Å allows us to include 40 chains in the simulation, and finite-size effects are then negligible for the wavevectors of interest. It is clear that a treatment of longer chains would not only require larger box sizes but also much longer runs, and therefore is very difficult. We also emphasize that equation (6) is not a good basis to describe interactions between chemically dissimilar polymers with sufficient accuracy.

2. MD algorithms and some simulation 'knowhow'

2.1. Classical mechanics and the Verlet algorithm

We consider a system of N particles (atoms) with Cartesian coordinates $\vec{X} = \{\vec{r}_i\}$, $i = 1, \ldots, N$, in a d-dimensional space. The dynamics then is described by Newton's equations of motion,

$$m_i \ddot{\vec{r}}_i = -\frac{\partial U_{\text{pot}}}{\partial \vec{r}_i} = \vec{f}_i, \tag{7}$$

m_i being the mass of the ith particle, and $\vec{f}_i$ the force acting on it, which we assume to be entirely due to interactions with other particles. Thus, the potential $U_{\rm pot}(\vec{X}) = U_{\rm pot}(\vec{r}_1, \ldots, \vec{r}_N)$ is written as

$$U_{\rm pot} = \sum_{i=1}^{N-1} \sum_{j>i}^{N} U(\vec{r}_{ij}), \qquad \vec{r}_{ij} = \vec{r}_i - \vec{r}_j, \tag{8}$$

where in the last step we have furthermore made the simplifying assumption that $U_{\rm pot}$ is pairwise additive (this assumption, which is reasonable for simple liquids, is not really necessary: it can be generalized whenever appropriate; we only make it for the sake of simplicity of our presentation). Thus

$$\vec{f}_i = -\sum_{j(\neq i)} \partial U(r_{ij})/\partial \vec{r}_i = \sum_{j(\neq i)} \vec{f}_{ij}. \tag{9}$$

The total energy

$$E = E_{\rm kin} + U_{\rm pot} = \sum_{i=1}^{N} \tfrac{1}{2} m_i \dot{\vec{r}}_i^{\,2} + U_{\rm pot} \tag{10}$$

is a constant of motion,

$$\frac{{\rm d}E}{{\rm d}t} = \sum_{i=1}^{N} m_i \dot{\vec{r}}_i \ddot{\vec{r}}_i - \sum_{i=1}^{N} \dot{\vec{r}}_i \cdot \vec{f}_i = 0. \tag{11}$$

MD now means that Newton's equations of motion are integrated numerically. A computationally efficient scheme is the so-called Verlet algorithm [38]. To derive it, we expand $\vec{r}_i(t)$ forward and backward in time,

$$\vec{r}_i(t+\delta t) = \vec{r}_i(t) + \delta t \vec{v}_i(t) + \frac{1}{2m_i}(\delta t)^2 \vec{f}_i(t) + \frac{1}{6}(\delta t)^3 \vec{b}_i(t) + {\rm O}((\delta t)^4), \tag{12}$$

$$\vec{r}_i(t-\delta t) = \vec{r}_i(t) - \delta t \vec{v}_i(t) + \frac{1}{2m_i}(\delta t)^2 \vec{f}_i(t) - \frac{1}{6}(\delta t)^3 \vec{b}_i(t) + {\rm O}((\delta t)^4). \tag{13}$$

Here $\vec{v}_i(t)$ is the velocity of the ith particle at time t, and $\vec{b}_i(t)$ is the corresponding vector that appears in the third order of the Taylor expansion.

For $\ddot{\vec{r}}(t)$ we have already substituted Newton's equation. Adding both expansions, the odd terms cancel, and hence

$$\vec{r}_i(t+\delta t) = 2\vec{r}_i(t) - \vec{r}_i(t-\delta t) + \frac{1}{m_i}(\delta t)^2 \vec{f}_i(t) + {\rm O}((\delta t)^4). \tag{14}$$

Subtraction of the expansions yields the velocity

$$\vec{v}_i(t) = \frac{1}{2(\delta t)}[\vec{r}_i(t+\delta t) - \vec{r}_i(t-\delta t)] + {\rm O}((\delta t)^3). \tag{15}$$

This Verlet algorithm [1, 7, 19, 37, 38] is manifestly time reversible: exchange of $\vec{r}_i(t+\delta t)$ and $\vec{r}_i(t-\delta t)$ yields the propagator for the time evolution going backward in time, and changes the sign of the velocity.

A peculiarity of the Verlet algorithm is the fact that the updating of the velocities is one step behind: the velocities at time t can only be calculated, see equation (15), after the positions at time $t+\delta t$ have become available. The updating of positions and velocities is synchronized in the 'velocity Verlet algorithm' [40]. Using

$$\vec{r}_i(t+\delta t) = \vec{r}_i(t) + \delta t \vec{v}_i + \frac{1}{2m_i}(\delta t)^2 \vec{f}_i(t) \tag{16}$$

together with the corresponding time-reversed equation

$$\vec{r}_i(t) = \vec{r}_i(t+\delta t) - \delta t \vec{v}_i(t+\delta t) + \frac{1}{2m_i}(\delta t)^2 \vec{f}_i(t+\delta t) \tag{17}$$

one obtains by adding these equations

$$\vec{v}_i(t+\delta t) = \vec{v}_i(t) + \frac{\delta t}{2m_i}[\vec{f}_i(t) + \vec{f}_i(t+\delta t)]. \tag{18}$$

The propagation of the velocities hence requires that both the forces of the present and the future configurations are known. The second set of forces can be determined as soon as the coordinates at time $t+\delta t$ have been obtained. Note that both the Verlet and the velocity Verlet algorithms are completely equivalent: they produce identical trajectories.

At this point it is of interest to ask what is the scale for the time step. For simplicity we consider liquid argon, the 'fruit fly' for MD. The argon atoms are assumed to interact with an LJ potential as considered in equation (6), with parameters $\sigma \approx 3.4$ Å, $\varepsilon/k_B \approx 120$ K and $m \approx 6.6 \times 10^{-23}$ g. Rescaling coordinates by writing $\vec{r}^* \equiv \vec{r}/\sigma$, we obtain

$$\vec{r}^*(t+\delta t) = 2\vec{r}^*(t) - \vec{r}^*(t-\delta t) - (\delta t)^2 \frac{48\varepsilon}{m\sigma^2} \frac{\vec{r}^*_{ij}}{|\vec{r}^*_{ij}|} \sum_{j(\neq i)} [(r^*_{ij})^{-13} - (r^*_{ij})^{-7}/2]. \tag{19}$$

From this equation we see that the natural time unit τ_0 is

$$\tau_0 = \left(\frac{m\sigma^2}{48\varepsilon}\right)^{1/2}, \tag{20}$$

which is roughly $\tau_0 \approx 3.1 \times 10^{-13}$ s for argon. In order to keep numerical integration errors small, we need to choose the time step δt so small that the third term on the rhs of equation (19) is significantly smaller than the first and second terms. For the LJ system this usually means $\delta t^* = 0.03$, which translates into real time units $\delta t \approx 10^{-14}$ s for the time step. So even with a million time steps (rescaled time $t^* = t/\tau_0 = 30\,000$) one only reaches a real time of about 10 ns.

It is also useful to go beyond this 'pedestrian approach' to classical mechanics, discussing more formally the time evolution in phase space, combining the Cartesian coordinates of all the particles ($\vec{X}$) and their momenta $\vec{P} = (\vec{p}_1, \vec{p}_2, \ldots, \vec{p}_N)$ into a point in a $2Nd$-dimensional space, $\Gamma \equiv (\vec{X}, \vec{P})$. Liouville's theorem says that the flow in phase space has the property that it is incompressible, phase space volume is conserved. One can formally write for any observable A

$$A(\Gamma, t) = \hat{U}(t) A(\Gamma, 0), \tag{21}$$

where the propagator $\hat{U}(t)$ is a unitary operator,

$$\hat{U}(t) = \exp(\mathrm{i}\hat{\mathcal{L}}t), \tag{22}$$

$\hat{\mathcal{L}}$ being the Liouville operator. Now the Verlet algorithm has the desirable feature that (to order $(\delta t)^3$) unitarity is preserved. This fact may to some extent explain why the Verlet algorithm is such a particularly stable algorithm over very long times (for a detailed discussion of the stability of the Verlet algorithm see [41]).

2.2. Estimation of intensive thermodynamic variables; the NVT ensemble

If the energy E were rigorously conserved by the algorithm it would realize states distributed according to the microcanonical (NVE) ensemble of statistical mechanics. Of course due to integration errors the energy is not strictly conserved and hence one has to make sure that the

chosen time step is small enough, as will be discussed below—let us disregard this problem for the moment and assume that the microcanonical ensemble is realized perfectly. How do we then estimate the thermodynamic variables of interest, such as temperature T and pressure p?

One can make use of the fact that in classical statistical mechanics the distributions of positions and velocities factorize; one simply has a Maxwell–Boltzmann distribution for the velocities and thus T can be inferred from the kinetic energy of the particles. Defining a 'kinetic temperature' $\mathcal{T}$ as follows (for $d = 3$)

$$\mathcal{T} = \frac{2}{3k_B N} E_{\rm kin} = \frac{1}{3k_B N} \sum_{i=1}^{N} m_i \vec{v}_i^2, \tag{23}$$

the desired estimate of the temperature of the system is then computed as the average $T = \langle \mathcal{T} \rangle$. It must be emphasized that for finite N in the microcanonical ensemble there occur fluctuations in temperature, described by [42]

$$\frac{[\langle \mathcal{T}^2 \rangle - \langle \mathcal{T} \rangle^2]}{\langle \mathcal{T} \rangle^2} = \frac{2}{3N} \left(1 - \frac{3k_B}{2C_v} \right), \tag{24}$$

where C_v is the specific heat of the system (at constant volume). Considering that one always works with a finite length of the MD run, these fluctuations cause a statistical error in the estimation of the temperature.

The pressure p can be estimated using the virial theorem. The dynamical variable whose average yields the pressure is defined as

$$\mathcal{P} = \frac{1}{3V} \left(2E_{\rm kin} + \sum_{i=1}^{3N} \vec{r}_i \cdot \vec{f}_i \right), \tag{25}$$

such that

$$p = \langle \mathcal{P} \rangle = \frac{N k_B T}{V} + \frac{1}{3V} \sum_{i=1}^{N} \langle \vec{r}_i \cdot \vec{f}_i \rangle. \tag{26}$$

Now we return to the problem that the energy is not strictly conserved by the algorithm described so far. The original recipe used in early MD work was to rescale the velocities from time to time such that one corrects for the drift in the energy. Alternatively, one can draw randomly velocities from time to time from a Maxwell–Boltzmann distribution. Both methods have the disadvantage that dynamic correlations are somewhat disturbed, and one realizes in this way neither a microcanonical nor a canonical ensemble. In the canonical (NVT) ensemble, temperature is a given variable and therefore not fluctuating at all, and instead of the fluctuations of $\mathcal{T}$ (equation (24)) one encounters fluctuations of the total energy E, described by another fluctuation relation:

$$N C_v / k_B = (1/k_B T)^2 (\langle \mathcal{H}^2 \rangle_{NVT} - \langle \mathcal{H} \rangle_{NVT}^2). \tag{27}$$

Here $\mathcal{H}$ is the Hamiltonian of the system. With methods in which one rescales the velocities, both temperature and energy are fluctuating, and neither equation (24) nor (27) hold.

However, one can introduce an MD method that does reproduce the canonical (NVT) ensemble exactly: one has to extend the Lagrangian of the system by a variable, representing the thermostat which has a fictitious mass Q. This yields the Nosé–Hoover algorithm [43, 44]. Newton's equations of motion are then extended by a 'friction' term,

$$\ddot{\vec{r}}_i = \vec{f}_i / m_i - \zeta \dot{\vec{r}}_i. \tag{28}$$

The friction coefficient $\zeta(t)$ fluctuates in time around zero, according to the equation

$$\dot{\zeta} = \frac{1}{Q} \left[\sum_{i=1}^{N} m_i \vec{v}_i^2 - 3N k_B T \right]. \tag{29}$$

Thus, $\zeta(t)$ responds to the imbalance between the instantaneous kinetic energy and the intended canonical average (remember $\sum_i m_i\langle\vec{v}_i^2\rangle = 3Nk_BT$). Although the total energy is no longer conserved, one can identify a conserved energy-like quantity $\mathcal{H}'$,

$$\mathcal{H}' = \mathcal{H} + \tfrac{1}{2}Q\zeta^2 + 3Nk_BT\int \zeta(t')\,\mathrm{d}t', \tag{30}$$

for which one can show that $\mathrm{d}\mathcal{H}'/\mathrm{d}t = 0$.

In this case also it is true that dynamical correlation functions between observables such as $\langle A(0)A(t)\rangle$ are not precisely identical to the microcanonical ones. However, in many cases of practical interest (e.g., dense systems of flexible bead–spring-type chain molecules representing a glass-forming polymer melt [45]) the difference between the result for $\langle A(0)A(t)\rangle$ from a strictly microcanonical run and a run using this Nosé–Hoover thermostat is negligibly small [45].

It is also possible to realize the isothermal–isobaric (NpT) ensemble, where the pressure is given and rather the volume fluctuates, by coupling to the so-called 'Andersen barostat' [46]. We shall not describe this here, but refer the reader to the literature [1, 7, 39] for details.

2.3. Diffusion, hydrodynamic slowing down and the Einstein relation

As a final point of this discussion of technical aspects, let us discuss how one extracts diffusion constants and other transport coefficients from MD simulations. We consider first the phenomenological description of diffusion in a single-component system in terms of Fick's law since this will allow us to discuss concepts such as hydrodynamic slowing down, the Einstein relation for the diffusion coefficient D in terms of mean square displacements of particles, and the Green–Kubo formula providing a link with the velocity autocorrelation function [1, 19, 47].

Fick's law states that there is a current of particles caused if there is a (particle) density gradient (or a gradient in the concentration) and this current acts to reduce the gradient. For small and slow density variations this is a linear relation,

$$\vec{j}(\vec{r},t) = -D\nabla\rho(\vec{r},t), \tag{31}$$

where D is the diffusion constant. If we combine this (phenomenological!) constitutive equation of irreversible thermodynamics with the (exact!) continuity equation which expresses the fact that the total particle number N is conserved,

$$\partial\rho(\vec{r},t)/\partial t + \nabla\cdot\vec{j}(\vec{r},t) = 0, \tag{32}$$

we get the well known diffusion equation,

$$\partial\rho(\vec{r},t)/\partial t = D\nabla^2\rho(\vec{r},t). \tag{33}$$

This equation is easily solved both in real space and in reciprocal space. In reciprocal space a simple exponential relaxation of the Fourier components of the density fluctuations $\delta\rho_{\vec{k}}(t)$ results,

$$\delta\rho(\vec{r},t) = \rho(\vec{r},t) - \langle\rho\rangle = \int \delta\rho(\vec{k},t)\exp(\mathrm{i}\vec{k}\cdot\vec{r})\,\mathrm{d}\vec{k}, \tag{34}$$

since

$$\frac{\mathrm{d}}{\mathrm{d}t}\delta\rho(\vec{k},t) = -Dk^2\delta\rho(\vec{k},t), \qquad \delta\rho(\vec{k},t) = \delta\rho(\vec{k},0)\exp(-Dk^2t). \tag{35}$$

We recognize that the associated relaxation time $\tau_{\vec{k}}$ diverges as $k \to 0$,

$$\tau_{\vec{k}} = (Dk^2)^{-1}. \tag{36}$$

Therefore we see that the dynamic correlation function of density fluctuations for long wavelengths in a diffusive system decays very slowly,

$$S(\vec{k},t) \equiv \langle \delta\rho(-\vec{k},0)\delta\rho(\vec{k},t)\rangle = S(k)\exp(-Dk^2t), \tag{37}$$

where $S(k)$ is the static structure factor from equation (1): $S(k) = \langle \delta\rho(-\vec{k},0)\delta\rho(\vec{k},0)\rangle$. Equations (36) and (37) demonstrate the so-called 'hydrodynamic slowing down' [48]. On the one hand, analysis of the intermediate scattering function as given by equation (37) allows us to extract the diffusion constant. On the other hand, this hydrodynamic slowing down is a difficulty for equilibration in the NVT ensemble, *both* for MD and for MC simulations. Remember that for the simulations of fluids, it is often convenient to use as an initial state a regular arrangement of the particles in the box, by simply putting them on the sites of the crystal lattice. This implies that $S(k \to 0) = 0$ in the initial state. If the simulated volume is large, so that the smallest wavevector $k_{\min} = 2\pi/L$ is small, it will take a very long time until $S(k_{\min})$ reaches its equilibrium value. In judging whether or not full equilibrium has been achieved, one hence cannot rely on the recipe advocated in some of the early simulation literature to check whether the internal energy has reached its equilibrium value. This was OK for the early work, where only 64 or 256 particles were simulated, and hence $k_{\min}$ was not small. Being interested in the simulation of much larger systems today, the issue of equilibrating long wavelength fluctuations properly needs careful consideration [49].

It is also useful to examine the diffusion equation in real space since it readily allows us to derive the Einstein relation for the mean square displacement of a diffusing particle. Let us take as an initial condition for the solution of equation (33) a δ-function, $\rho(\vec{r},t=0) = \delta(\vec{r}-\vec{r}_0)$ (note that the normalization $\int \rho(\vec{r},t)\,\mathrm{d}\vec{r} = 1$ means that $\rho(\vec{r},t)$ can be interpreted physically as the conditional probability of finding a particle at $\vec{r}$ after a time t provided this particle was at $\vec{r} = \vec{r}_0$ at time $t = 0$). Now the solution of equation (33) is simply a Gaussian distribution,

$$\rho(\vec{r},t) = (4\pi Dt)^{-d/2}\exp[-(\vec{r}-\vec{r}_0)^2/(4Dt)], \tag{38}$$

d denoting once more the dimension of space. The squared half width of this distribution increases linearly with time t, and so does the mean square displacement:

$$\langle[\delta\vec{r}(t)]^2\rangle = \langle[\vec{r}(t)-\vec{r}_0]^2\rangle = 2dDt, \qquad t \to \infty. \tag{39}$$

We have added here the restriction to consider large times ($t \to \infty$) since then this Einstein relation, equation (39), holds quite generally, while typically the simple diffusion equation, equation (33), will not hold on small length scales (of the order of a few atomic diameters or less) and the corresponding short times. This fact will be evident with the examples discussed later. In fact, equation (39) is routinely used in simulations to compute the (self-)diffusion constants.

2.4. Green–Kubo relations and transport coefficients

It is also interesting to note that there is a relation between the self-diffusion constant and the velocity autocorrelation function of a diffusing particle [19].

Writing

$$\vec{r}(t) - \vec{r}_0 = \int_0^t \vec{v}(t')\,\mathrm{d}t', \tag{40}$$

the mean square displacement can be expressed as follows:

$$\langle[\vec{r}(t)-\vec{r}_0]^2\rangle = \int_0^t \mathrm{d}t' \int_0^t \mathrm{d}t''\,\langle\vec{v}(t'')\cdot\vec{v}(t')\rangle = d\int_0^t \mathrm{d}t' \int_0^t \mathrm{d}t'' Z(t''-t'), \tag{41}$$

with $Z(t''-t') \equiv \langle v_\alpha(t'')v_\alpha(t')\rangle$. In this notation, we imply that in equilibrium translation invariance holds, so Z depends only on the time difference $t''-t'$, not on the two times t', t'' separately. v_α is one of the d Cartesian components of $\vec{v}$. Rearranging the domain of integration in equation (41) readily yields

$$\langle[\vec{r}(t)-\vec{r}_0]^2\rangle = 2\,\mathrm{d}t\int_0^t (1-s/t)Z(s)\,\mathrm{d}s \underset{t\to\infty}{\longrightarrow} 2dDt, \tag{42}$$

with

$$D = \int_0^\infty Z(s)\,\mathrm{d}s = \int_0^\infty \langle v_\alpha(0)v_\alpha(t)\rangle\,\mathrm{d}t. \tag{43}$$

This result that the self-diffusion constant is the time integral of the velocity autocorrelation function is a special case of a 'Green–Kubo relation' [19]. Another example of such a relation is that the shear viscosity η is related to time correlations of the off-diagonal components of the pressure tensor σ_{xy},

$$\eta = \frac{1}{Vk_BT}\int_0^\infty \mathrm{d}t\,\langle\sigma_{xy}(0)\sigma_{xy}(t)\rangle, \tag{44}$$

where

$$\sigma_{xy} = \sum_{i=1}^N \left\{ m_i v_i^x v_i^y + \tfrac{1}{2}\sum_{j(\neq i)} x_{ij} f_y(r_{ij}) \right\}, \tag{45}$$

f_y being the y-component of the force with which particles i, j interact, $f_y = -\partial U(r_{ij})/\partial y$, cf equation (9), $\vec{r}_{ij} = \vec{r}_i - \vec{r}_j$. Similarly, for the thermal conductivity λ_T we need to consider correlations of the energy current density [19, 47]

$$\lambda_T = \frac{1}{Vk_BT^2}\int_0^\infty \mathrm{d}t\,\langle j_z^e(0)j_z^e(t)\rangle, \tag{46}$$

$$j_z^e = \frac{\mathrm{d}}{\mathrm{d}t}\left[\sum_{i=1}^N z_i\left(\frac{1}{2}m_i\vec{v}_i^2 + \sum_{j(\neq i)} U(r_{ij})\right)\right]. \tag{47}$$

Finally, the electrical conductivity σ_{el} can be obtained from correlations of the current density J_x^{el} of the electrical charges q_i [19, 47]

$$\sigma_{\mathrm{el}} = \frac{1}{Vk_BT}\int_0^\infty \mathrm{d}t\,\langle J_x^{\mathrm{el}}(0)J_x^{\mathrm{el}}(t)\rangle, \tag{48}$$

$$J_x^{\mathrm{el}} = \sum_{i=1}^N q_i v_i^x. \tag{49}$$

All these relations are in fact useful for MD simulations.

3. Application to the example of molten silica

As an example for the type of result that we can get using the Einstein and Green–Kubo relations that were just discussed, we show in figure 3 an Arrhenius plot for the viscosity of molten SiO_2 [50], and compare the MD results with experimental data [51]. 'Arrhenius plot' means the logarithm of the viscosity is plotted versus inverse temperature, since then an Arrhenius law ($\eta(T) \propto \exp[E_A/(k_BT)]$, where E_A is an 'activation energy'), shows up as a straight line in the plot, with a slope E_A. The experimental data included here [51] are indeed compatible with such a law. However, the extremely large values of the viscosity mean that the relaxation time of this melt is in the microsecond or even millisecond range. Therefore, the MD results cannot

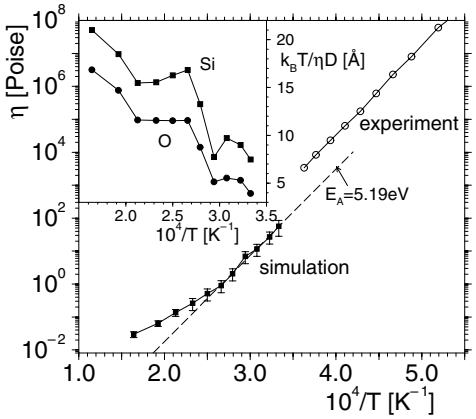

Figure 3. MD results (filled squares) for the viscosity of the BKS model for molten SiO_2 plotted versus inverse temperature. The dashed straight line indicates an Arrhenius fit with an activation energy $E_A = 5.19$ eV. The experimental data [51] (open circles) are compatible with this value but would suggest a slightly larger preexponential factor. Note that for SiO_2 the analysis of other correlation functions at very high temperature suggests a critical temperature $T_c = 3330$ K of mode coupling theory, therefore $\eta(T > T_c)$ deviates from the Arrhenius law. The inset shows that the Stokes–Einstein relation, $k_BT/(\eta D) =$ constant, where D are the Si or O self-diffusion constants, does not hold in the regime of temperatures studied (from [50]).

be obtained in the same temperature range where the experimental data were taken, but only at considerably higher temperatures, where experiments are no longer possible. Nevertheless, these simulation results (together with results for many other correlation functions [50] that will not be shown here) do have a great theoretical relevance, since they show that even SiO_2 has a regime of temperatures where the so-called mode coupling theory of the glass transition [52] can be applied. Since this regime of temperatures is inaccessible with laboratory experiments, the hypothesis was advanced that one needs several classes for glass-forming fluids with a fundamentally different dynamical behaviour. Figure 3 shows that 'computer experiments' can complement laboratory experiments by providing results for physical quantities in a parameter range which cannot be studied in the laboratory. Another interesting aspect of the data shown in figure 3 is that the Stokes–Einstein relation, linking the temperature dependence of the viscosity to that of the self-diffusion constant(s), does not hold.

Simulating real glass-forming fluids such as SiO_2 is difficult for various reasons: a great problem is again the choice of a suitable force field. In figure 3, the so-called BKS potential [53] was used, which has been proposed on the basis of quantum chemical calculations. It contains Coulomb-like interactions, but with effective charges $q_i\{i \in \mathrm{Si}, \mathrm{O}\}$ rather than the true ionic charges, and a short-range Buckingham potential,

$$U(r_{ij}) = \frac{q_i q_j e^2}{r_{ij}} + A_{ij}\exp(-B_{ij}r_{ij}) - C_{ij}/r_{ij}^6, \tag{50}$$

where e is the elementary charge, $q_0 = -1.2$, $q_{\mathrm{Si}} = +2.4$ and the constants A_{ij}, B_{ij} and C_{ij} can be found in the original reference [53]. It is somewhat surprising that a clever choice of these phenomenological constants allows us to describe the directional covalent bonding (typically a silicon atom is in the centre of a tetrahedron, with the oxygens at the corners), although one uses just pair potentials. Nevertheless, the simulations are still technically very difficult: the long-range Coulomb interaction necessitates the use of the time-consuming Ewald summation techniques [1–3]; the scale for the potential is in the electronvolt energy range and varies

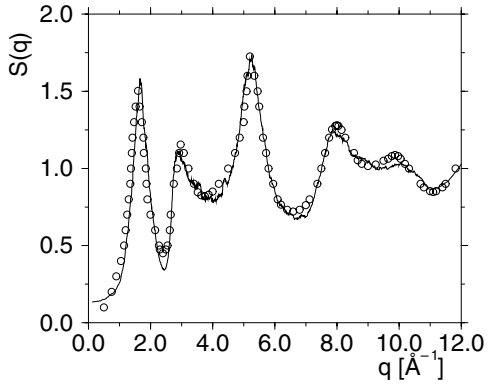

Figure 4. Static neutron structure factor of SiO_2 at room temperature ($T = 300$ K), plotted versus wavelength q. The full curve is the MD simulation [50], using the experimental scattering lengths for Si and O atoms, while the symbols are the neutron scattering data of Price and Carpenter [55] (from [50]).

rather rapidly with distance. Therefore one needs to use a rather small MD time step, namely $\delta t = 1.6$ fs.

If one produces amorphous glassy structures by an MD simulation with such a model, the most plausible procedure is the same as the one used in the glass factory. One starts at a very high temperature T_0, and then one cools the system gradually down at constant pressure, so the temperature $T(t)$ varies with time, e.g. $T(t) = T_0 - \gamma t$, γ being the cooling rate. While the structures obtained in this way look qualitatively reasonable [54], one must be aware of the fact that the cooling rates applied in the simulation are extremely large ($\gamma = 10^{12}$ K s^{-1} or even higher), which means that they are at least a factor 10^{12} larger than those used in the experiment. Thus, one must expect that the quantitative details of the results (including also the density of the material) will depend on the cooling rate distinctly, and this is what is actually found [54].

Better results are obtained if one proceeds in a slightly different way, where one no longer tries to predict the density of the model system from the simulation, but rather fixes it to the experimental value. The system is then carefully equilibrated at a 'moderately high' temperature before one cools it down to the desired temperature. 'Moderately high' for pure SiO_2 means $T = 2750$ K—then equilibration requires a run which is already 20 ns long. To avoid finite-size effects, a box of around 48 Å linear dimension needs to be taken, containing about 8000 atoms. This calculation requires substantial CPU resources (it was done [50] at a CRAY-T3E parallel supercomputer, performing force parallelization) so it is presently not easy to do much better.

In any case, with this procedure one does obtain the static structure factor of silica glass at room temperature in very good agreement with experiment. This can be inferred, e.g., from figure 4 where we show the static structure factor as measured in a neutron-scattering experiment, which is the weighted sum of the three partial static structure factors [19, 50, 51]. Since there are no adjustable parameters whatsoever involved in this comparison, this agreement is significant.

Figure 5 now shows an Arrhenius plot for the self-diffusion constants, using scales such that the experimental data [56, 57] can be included together with the simulation results. From this graph it becomes obvious that in principle one would like the simulation to span over 16 decades in dynamics, a task clearly impossible for MD. So there is again a gap between the

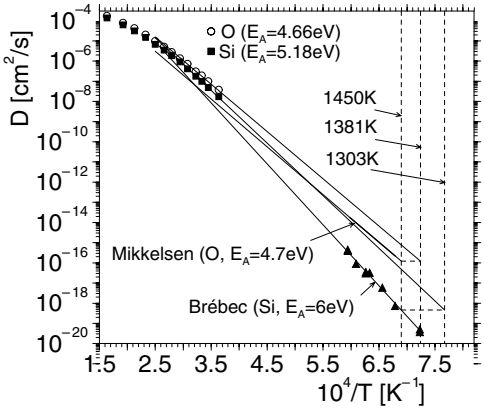

Figure 5. Plot of the self-diffusion constant D of silicon atoms (Si) and oxygen atoms (O) in molten SiO_2 as a function of inverse temperature. The symbols in the upper left part are the results from MD simulations and the data in the lower right part stem from experiments [56, 57]. The thin straight lines show simple Arrhenius behaviour ($D \propto \exp[-E_A/(k_B T)]$) with an activation energy E_A, as indicated in the figure. The vertical broken lines indicate the experimental glass transition temperatures, $T_g = 1450$ K, as well as values for T_g that one obtains if one extrapolates the data from the simulations to low temperatures and then estimates T_g from the experimental value of the O diffusion constant ($D_O(T = T_g^{sim}) = 10^{-16}$ cm^2 s$^{-1} \Longrightarrow T_g^{sim} = 1381$ K) or the Si diffusion constant, respectively ($D_{Si}(T = T_g^{sim}) = 5 \times 10^{-19}$ cm^2 s$^{-1} \Longrightarrow T_g^{sim} = 1303$ K) (from [50]).

range where simulations in thermal equilibrium are possible and the temperature range where the experimental data can be taken. But it is gratifying that the simulation can predict the activation energies for the self-diffusion constants almost correctly.

Now the real strength of the MD simulations is that one can record in a single calculation a great variety of different static and dynamic properties simultaneously. For instance, one can study the time dependence of autocorrelation functions of the generalized temperature fluctuation $\delta T_{\vec{q}}(t)$, which is the Fourier transform of the local 'temperature' $T(\vec{r}, t)$,

$$T(\vec{r}, t) = \sum_{i=1}^{N} \frac{\vec{p}_i^{\,2}}{3k_B m_i} \delta(\vec{r} - \vec{r}_i(t)). \tag{51}$$

One sees (figure 6(a)) [58] that for large wavelength q this correlator is rapidly relaxing but again one notes a slowing down at small q. This is another example of 'hydrodynamic slowing down'. Of course, the considerable statistical scatter of the results shown in figure 6(a) is somewhat disturbing. But it has to be mentioned that these results are already based on averages over 100–200 runs, corresponding to an effort of several years if one ran the problem on a single CPU, and hence it is currently difficult to do better.

Defining now from the time-displaced correlation function,

$$\Phi_{TT}(q, t) = \langle \delta T_{-\vec{q}}(0) \delta T_{\vec{q}}(t) \rangle, \tag{52}$$

a relaxation time τ by the condition

$$\Phi_{TT}(q, t = \tau) \equiv \Phi_{TT}(q, t = 0)/10, \tag{53}$$

one obtains the data shown in figure 6(b). Here a plot of τq^2 versus q^2 is presented, since theory predicts [58]

$$\tau = \frac{\rho C_p}{\lambda_T} \frac{1}{q^2} + \text{constant}, \tag{54}$$

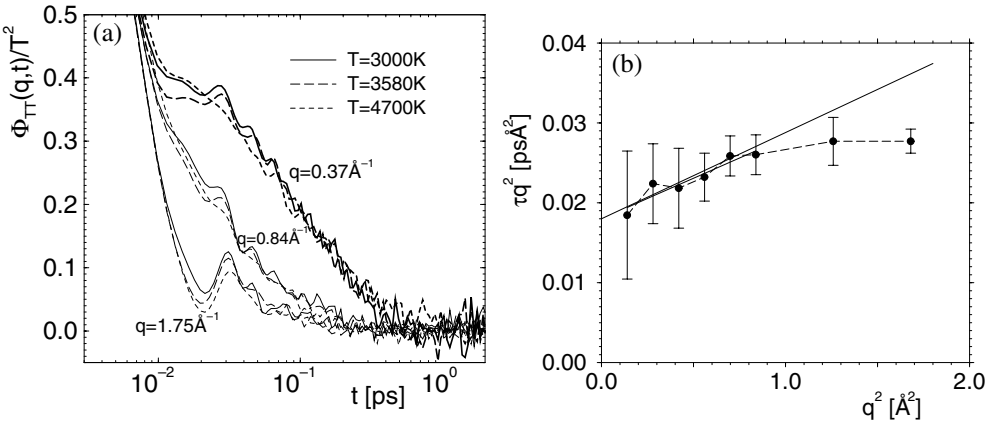

Figure 6. (a) Time dependence of the autocorrelation function $\Phi_{TT}(q,t)/T^2$ of the generalized temperature fluctuation $\delta T_q(t)$ for SiO_2, showing data for three temperatures T and three choices of wavevector q as indicated. All data refer to systems containing 224 oxygen and 112 silicon atoms. (b) Plot of wavevector squared times the relaxation time τ, as defined in equation (53), versus q^2. From the extrapolated intercept for $q^2 \to 0$, the estimate $\lambda_T \approx 2.4$ W K^{-1} m^{-1} for the thermal conductivity λ_T is extracted (from [58]).

where $\rho = N/V$ is the density, C_p the heat capacity and λ_T is the thermal conductivity. Since ρ is given and C_p can be estimated independently, one obtains a rough estimate of the thermal conductivity λ_T from these data (figure 6(b)). This estimate is in reasonable qualitative agreement with experiments, which indicate that for $T \geqslant 1000$ K λ_T is only weakly dependent on temperature and in the range $2 \leqslant \lambda_T \leqslant 3$ W K^{-1} m^{-1} [58].

As a last example, the temperature dependence of the longitudinal (c_ℓ) and the transverse (c_t) sound velocity is shown in figure 7 [59]. These results were obtained from an analysis of the corresponding time-displaced current–current correlation functions which were Fourier transformed into frequency space. Undamped propagation of sound manifests itself by δ-functions $\delta(\omega - \omega_q)$ with $\omega_q = c_{l,t}q$ for $q \to 0$ in these correlators [59]. Of course, in a liquid for $q \to 0$ no static shear can be maintained and hence in that case only c_ℓ is well defined. However, for not too small q both longitudinal and transverse correlators show broad peaks, and the positions of these peaks are shown in figure 7. Again one notes very nice agreement with corresponding experimental data [60].

4. A brief introduction to non-equilibrium molecular dynamics (NEMD)

Already in equation (31), we have considered the situation where the density in the system may deviate from its constant equilibrium value, and we have postulated a linear relation between the particle density current and the gradient of the local density $\nabla\rho(\vec{r}, t)$. Similarly, we can also assume that there is no longer complete thermal equilibrium, as far as the temperature is concerned, but only 'local equilibrium': we may still assume a Maxwell–Boltzmann velocity distribution of the particles but with a temperature $T(\vec{r}, t)$ that slowly varies in space. Thus, a current of energy, i.e. heat, is created, the coefficient between the temperature gradient and the energy current density being the thermal conductivity λ_T, yielding Fourier's law of heat conduction,

$$\vec{j}_Q = -\lambda_T[\nabla T(\vec{r}, t)]. \tag{55}$$

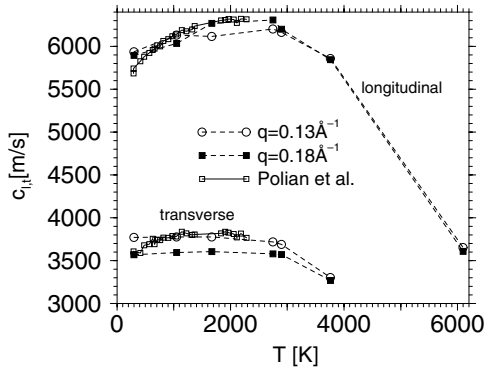

Figure 7. Longitudinal (c_ℓ) and transverse (c_t) sound velocities of SiO_2 plotted versus temperature. These quantities were determined from the frequency positions of the maxima of the corresponding longitudinal and transverse current correlation functions at $q = 0.13$ Å^{-1} (open circles) and $q = 0.18$ Å^{-1} (filled squares). Also included are the experimental data of Polian *et al* [60] which are multiplied with the factor $(2.2/2.37)^{1/2}$ since the simulation was done at a density of $\rho_{\rm sim} = 2.37$ g cm^{-2} while the experiment was done for $\rho_{\rm exp} = 2.2$ g cm^{-2} (from [59]).

Now in reality the situation is not so simple, since energy density and particle number density are coupled variables. Each gradient therefore also produces a current of the other variable. So we have to generalize the set of flow equations (31), (55) to a matrix form, involving the Onsager coefficients $\Lambda_{\alpha\beta}$,

$$\vec{j}_Q = \Lambda_{QQ}\nabla\left(\frac{1}{k_BT}\right) - \Lambda_{Qi}\nabla\left(\frac{\mu_i}{k_BT}\right), \tag{56}$$

$$\vec{j}_i = \Lambda_{iQ}\nabla\left(\frac{1}{k_BT}\right) - \Lambda_{ii}\nabla\left(\frac{\mu_i}{k_BT}\right), \tag{57}$$

with μ_i being the chemical potential of particle species i (the generalization of equations (56), (57) to systems containing several different species of particles is then obvious). Also, we have written the set of constitutive equations entirely in terms of gradients of intensive variables, rather than using the density of an extensive variable as in equation (31). Of course, using thermodynamics, the corresponding relation is easily established, since with equation (31) one obtains

$$\frac{\nabla\mu_i}{k_BT} = \left(\frac{\partial\mu_i}{\partial\rho_i}\right)_T \frac{1}{k_BT}\nabla\rho_i \Longrightarrow D_i = \frac{\Lambda_{ii}}{k_BT}\left(\frac{\partial\mu_i}{\partial\rho_i}\right)_T. \tag{58}$$

In NEMD simulations one usually sets up a stationary gradient by suitable boundary conditions creating a stationary current through the system. In the case of a flow of particles, this is clearly compatible with periodic boundary conditions: particles leaving the simulation box on the right simultaneously reenter on the left. For instance, we may confine a fluid between two parallel plates and let a constant force act on the particles [20, 21, 61–63] but schemes where one avoids external walls altogether are also possible [20, 21, 64]. In the latter case, one can obtain a homogeneous flow, while in the former case the velocity profile is inhomogeneous, and also the structure of the fluid close to the external walls is modified.

Now an important aspect of all such stationary flows is that entropy is produced: the entropy production per unit time is

$$\frac{{\rm d}s}{{\rm d}t} = \Lambda_{QQ}\left[\nabla\frac{1}{k_BT}\right]^2 + (\Lambda_{Qi} + \Lambda_{iQ})\left[\left(\nabla\frac{1}{k_BT}\right)\left(\frac{\nabla\mu_i}{k_BT}\right)\right] + \Lambda_{ii}\left[\frac{\nabla\mu_i}{k_BT}\right]^2. \tag{59}$$

Although this entropy production per unit time is small for small gradients, nevertheless the heat that is produced makes a strictly microcanonical simulation impossible: the system would heat up steadily. Thus one always has to use a thermostat.

As an example for such applications of NEMD, we now briefly review some results [62] obtained for a bead–spring model of short polymer chains confined between two parallel plates. The interaction between the beads is a simple LJ potential of the form as written in equation (6) (truncated at $r_c = 2.24\sigma$ and shifted so that $U(r = r_c) = 0$, as usual). The 'spring potential' between neighbouring effective monomeric units is taken to be the finitely extensible nonlinear elastic (FENE) potential,

$$U_{\mathrm{FENE}}(\ell) = -15R_0^2 \ln[1 - (\ell/R_o)^2] \tag{60}$$

choosing 'LJ units' for length, energy and temperature as usual, $\sigma = 1$, $\varepsilon = 1$, $k_B = 1$ (and also the mass of the effective monomers $m = 1$, which fixes the unit of time as well, cf equation (20)). Choosing $R_0 = 1.5$ one finds that the total bond potential (LJ + FENE) has its minimum at $\ell_0 \approx 0.96$, while the LJ potential has its minimum at $r_0 = 2^{1/6} \approx 1.13$. This competition between these two length scales prevents crystallization of this melt, and hence is the physical reason that this model is a very good model for a glass-forming polymer melt [45, 65]. Note that unlike the atomistic model [34, 35] discussed in section 1.3 of the present article, neither a bond angle potential nor a torsional potential is included in this case. In fact, one envisages that the 'effective monomers' are formed by combining a few subsequent chemical monomers along the backbone of the chain molecule into one such effective unit of a 'coarse-grained' model [8, 9, 28].

For a chain length $N = 10$ a box of linear dimensions $L_x \times L_y \times D$, with $L_x = L_y = 10.05$, $D = 20$, containing 200 chains in the system is a good choice [62]. We used periodic boundary conditions in x and y directions, while in the remaining z-direction one places walls formed by atoms on a triangular lattice, at equilibrium positions $\vec{r}_{i,\mathrm{eq}}$ with $z_{i,\mathrm{eq}} = \pm D/2$. These wall atoms are bound to their equilibrium positions with a harmonic potential, $U_{\mathrm{harm}}(\vec{r}_i) = \frac{1}{2}K_h(\vec{r}_i - \vec{r}_{i,\mathrm{eq}})^2$, with $K_h = 100$.

In order to represent the physical effect of the atoms in the (massive) walls other than those in the first layers of the wall, one coarse-grains them into an effectively repulsive background potential $U_{\mathrm{wall}}(z) = \varepsilon(\sigma/z)^9$, where $z \equiv |z_{\mathrm{mon}} - z_{\mathrm{wall}}|$, z_{mon} being the z-coordinate of the considered monomer, and $z_{\mathrm{wall}} = \pm(\sigma + D/2)$ the effective positions of the second layer on top of the walls. In order to create a flow in this geometry, a force $\vec{F}^e$ acts in the $+x$-direction on each monomer, and one also needs to specify the interaction between the monomers and the atoms in the top layers of the walls, which determine the 'hydrodynamic boundary conditions' of the resulting Poisseuille flow [20, 61–63].

In [62] this interaction was chosen of the same LJ form as the interaction between non-bonded effective monomers, but with different parameters, $\sigma_{\mathrm{wm}} = 2^{-1/6}$, $\varepsilon_{\mathrm{wm}} = 2$. In this way one creates a 'stick' boundary condition for the flow, while for $\sigma_{\mathrm{wm}} = 1$, $\varepsilon_{\mathrm{wm}} = 1$ one would have a strong partial slip, and the estimation of transport coefficients from the velocity and temperature profiles would be more difficult.

Figure 8 shows typical results for the density and velocity profile across the slit. One can recognize a very pronounced 'layering' phenomenon near both walls, i.e. $\rho(z)$ exhibits very strong oscillations, but these oscillations are only weakly dependent on temperature, and furthermore in the centre region of the thin polymer film ($-5 \leqslant z \leqslant +5$) the density profile is essentially flat, exhibiting the behaviour of the bulk. Using the radial distribution function $g(\vec{r})$, with a vector $\vec{r}$ parallel to the walls, it has been checked that the system still has a fluid-like structure (and not crystallized, for instance) near the walls where the strong layering phenomena occurs.

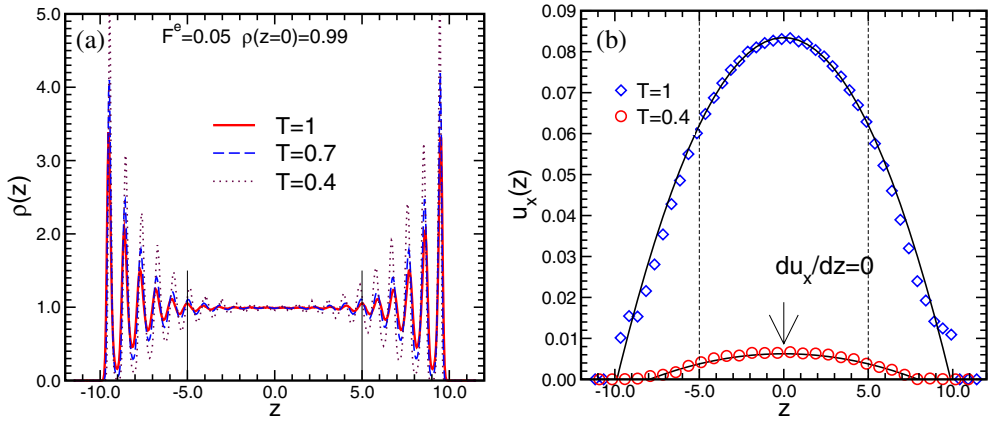

Figure 8. (a) Monomer density profiles of a polymer melt confined in a slit. The bulk density is $\rho = \rho(z = 0) = 0.99$ and the amplitude of the force in the x-direction is $F^e = 0.05$. Three temperatures are included as indicated. Note that the coordinate origin for the z-axis is chosen in the centre of the polymer film. (b) Velocity profile $u_x(z)$ for two temperatures (as indicated) and otherwise the same conditions as in panel (a). The parabolic curves indicate the fitted Poisseuille flow profiles, equation (61) (from [62]).

The central region ($-5 \leqslant z \leqslant +5$) is then used to fit the Poisseuille-type flow profile (well known from hydrodynamics) to the data, i.e. [66]

$$u_x(z) = -\rho_0 F^e (z^2 - z_{\text{wall}}^2 - 2z_{\text{wall}}\delta)/\eta, \tag{61}$$

where $\rho_0 = \rho\ (z = 0)$ is the bulk density, and δ has the physical interpretation of a slip length (note $\partial u_x(z)/\partial z|_{z=z_{\text{wall}}} = u_x(z = z_{\text{wall}})/\delta$). Figure 8(b) shows that excellent fits to equation (61) are in fact obtained, thus yielding an estimate of the viscosity η.

At this point a comment on how the thermostatting is done is in order. The most natural way (used in the laboratory experiments) would be to enforce isothermal conditions through the walls, keeping them at constant temperature by coupling the wall atoms to a thermostat. The heat created in the centre of the polymer film through the viscous flow then leads to a stationary temperature profile, and along the resulting temperature gradients the heat is transported towards the walls. Of course, if the viscous flow is too fast (when the force amplitude F^e is too large) one enters a regime of very nonlinear response, with strong temperature variations and large gradients, and then descriptions based on linear irreversible thermodynamics (equations (31), (51)–(61)) are not really applicable in a strict sense. As an example, figure 9 shows temperature profiles across the film observed in a simulation of this type. One sees that for $F^e \geqslant 0.1$ the temperature in the centre of the film is strongly enhanced, and one needs to choose $F^e \leqslant 0.05$ to stay within the linear response regime. Of course, the study of nonlinear phenomena far from equilibrium (such as 'shear thinning' [21], the decrease of the effective viscosity η_{eff} with increasing shear rate) may be of interest in itself, but this is outside the consideration here.

Figure 9 also demonstrates that the temperature profiles can also be fitted to the theoretical profiles resulting from the solutions of the phenomenological hydrodynamic equations [66, 67]

$$T(z) = T_{\text{wall}} + \frac{(\rho_0 F^e D^2)^2}{192\lambda_T \eta}\left[1 - \left(\frac{2z}{D}\right)^4\right]. \tag{62}$$

In the temperature range of figure 9, one obtains $3 \leqslant \lambda_T \leqslant 4.4$ as a result for the thermal conductivity. We also note that the data shown in figure 9 do not give any evidence for an

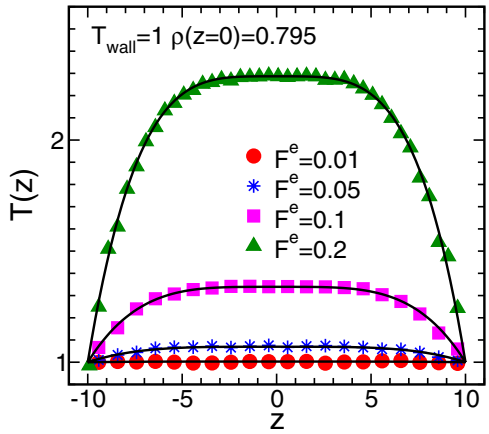

Figure 9. A comparison of the temperature profiles resulting from NEMD simulations (symbols) with the theoretical prediction equation (62) (curves) for various values of F^e at a wall temperature $T_{\rm wall} = 1$ and a bulk density $\rho(z = 0) = 0.795$. Contrary to the results shown in figures 8 and 10, here the fluid particles were not coupled to a heat bath but obeyed pure Newtonian dynamics, while the walls were thermostatted. Note that in computing the local temperature at z the streaming velocity $\vec{u}(z)$ is subtracted from the instantaneous velocities of all particles in the interval $[z, z+{\rm d}z]$ (from [62]).

additional term not included in Fourier's law, equation (55), namely a strain rate coupling that would lead to an additional quadratic term $\{\propto -(2z/D)^2\}$ in equation (62) [61].

Since in a glass forming fluid the viscosity is strongly temperature dependent, already a small variation of $T(z)$ across the film creates problems for the use of equation (62) at low temperature. It thus is preferable to apply the thermostatting algorithm not only to the wall atoms, but also to the fluid atoms, noting that in the presence of the flow the temperature is defined as $T = m\langle(\vec{v} - \langle\vec{v}\rangle)^2\rangle/3k_B$ instead of $T = \langle\mathcal{T}\rangle$ (equation (23)). Since here $\langle\vec{v}\rangle = (u_x(z), 0, 0)$, one has during the equilibration to determine the profile $u_x(z)$ self-consistently [62].

Figure 10 shows the result for the shear viscosity η and the lateral self-diffusion constant $D_\perp$ (obtained from mean square displacements in the y-direction perpendicular to the flow). One sees that one can obtain rather precise results for η and monitor the increase of η over about two decades. Both η and $D_\perp$ can be fitted well by the Vogel–Fulcher–Tammann (VFT) [65] relation,

$$\eta(T) = \eta(\infty)\exp[E_\eta/(T - T_0)], \qquad D_\perp = D(\infty)\exp[-E_D/(T - T_0)], \tag{63}$$

where the VFT temperature T_0 is the same for both quantities, while the effective activation energies E_η, E_D are slightly different. This difference is consistent with a direct examination of the ratio $\ell = k_B T/(4\pi D_\perp \eta)$, which should be a characteristic constant length if the Stokes–Einstein relation holds (cf figure 3): similarly as for SiO_2, one finds a systematic decrease of this ratio as the temperature gets lower [62].

5. Concluding comments

In this brief review, we have attempted to convey to the reader the flavour of MD simulations, addressing both the estimation of equilibrium properties such as static structure factors (figure 4) or density profiles near confining walls (figure 8(a)) and of dynamic properties,

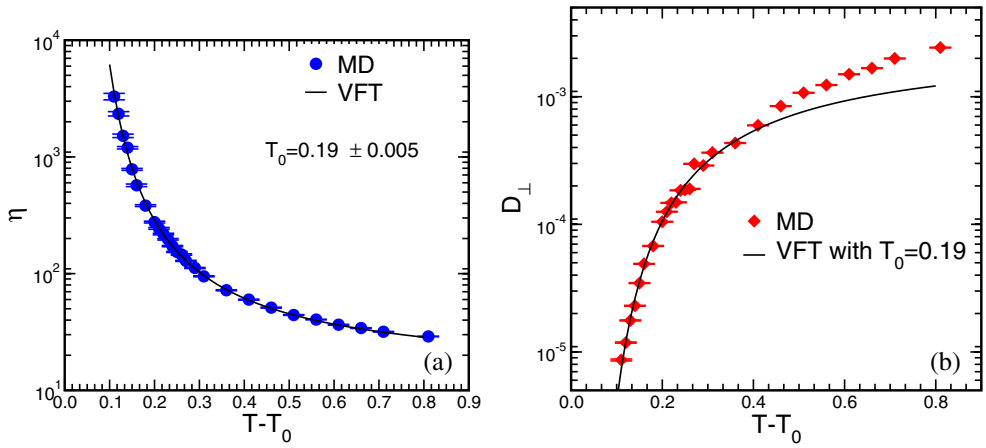

Figure 10. (a) Shear viscosity of the model polymer melt as a function of the temperature distance $T - T_0$ from the VFT temperature $T_0 = 0.190 \pm 0.005$. Symbols denote the data obtained for constant density $\rho_0 = 0.99$. The curve is a fit to the VFT equation (equation (63)). (b) The same as (a) but for the self-diffusion constant $D_\perp$ (measured in the y-direction transverse to the flow) (from [62]).

such as single-chain intermediate dynamic structure factors in polymer melts (figures 1 and 2), diffusion constants in SiO_2 (figure 5) and glass forming polymer melts (figure 10(b)), and collective transport coefficients such as viscosity (figures 3 and 10(a)), thermal conductivity etc. Both types of MD simulation, dealing with systems in thermal equilibrium and NEMD, has been discussed (section 4).

Already with respect to static properties, one has the choice between different ensembles (microcanonical NVE ensemble, or NVT and NpT ensembles, realized with suitable thermostats and barostats). Which ensemble is most appropriate depends on the questions which one would like to answer. Similarly, we have demonstrated that transport coefficients (such as viscosity, thermal conductivity etc) can be estimated from thermal equilibrium simulations (via the Green–Kubo [68] relations of section 2.4) or via NEMD work. There are many variants of how one can proceed [20, 21, 58–64, 67], and clearly there is no full consensus in the literature about the 'pros' and 'cons' of the various approaches yet. Instead the subject is still a matter of current research. Figure 11 presents an example, again SiO_2, where viscosities were estimated from an NEMD approach in complete analogy with figure 8(b), and the data are compared to the Green–Kubo approach used in figure 3. At least within the error bars noted in figure 3, there is very good mutual agreement, and this is reassuring because it shows that the various systematic errors of the simulations and their analysis are under control. We have emphasized that one must be aware of systematic errors due to the finite size of the simulation box, due to incomplete equilibration, in particular in the case of long-wavelength fluctuations, due to inaccuracies of the algorithm related to the size of the time step etc.

Finally, we emphasize that we have used illustrative examples which were taken from the research of the present authors for the sake of simplicity only—similarly valuable research on related problems is available in the literature from many other groups, as is well documented (see e.g. [1–3, 7, 19–21]). We hope that the present article 'whets the appetite' of the reader to study this extensive literature.

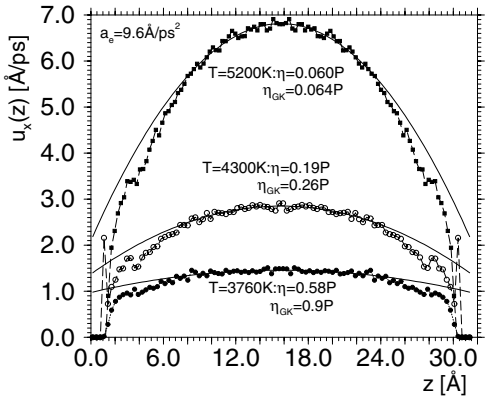

Figure 11. Velocity profile of molten SiO_2 between atomistic walls, for an acceleration $a_x = 9.6$ Å ps^{-2}, and three temperatures as indicated. Points are NEMD data using a simulation box $L_x \times L_y \times D$, with $L_x = L_y = 23.0$ Å, $D = 31.5$ Å, using altogether $N = 1152$ atoms. Curves are fits to equation (61). The resulting viscosities are quoted in the figure, together with the corresponding Green–Kubo estimates η_{GK} from [50] (from [63]).

Acknowledgments

The research reviewed here was supported by the Bundesministerium für Bildung und Forschung (BMBF No 03N6500 and 03N6015), by the Deutsche Forschungsgemeinschaft (DFG), grants SFB/262/D1, D2, HO2231/2-1 and by Schott Glas. We are very grateful to J Baschnagel, C Bennemann, A Latz, P Scheidler, G D Smith and K Vollmayr-Lee for their valuable collaboration on the research projects from which these examples were taken. Generous grants of computing time by the computer centre of the University of Mainz (ZDV) and on the CRAY-T3E from NIC Jülich and HLRS Stuttgart also is acknowledged.

References

[1] Allen M P and Tildesley D J 1987 *Computer Simulation of Liquids* (Oxford: Clarendon)
[2] Binder K and Ciccotti G (ed) 1996 *Monte Carlo and Molecular Dynamics of Condensed Matter Systems* (Bologna: Societá Italiana di Fisica)
[3] Frenkel D and Smit B 1996 *Understanding Molecular Simulation: From Algorithms to Applications* (San Diego, CA: Academic)
[4] Landau D P and Binder K 2000 *A Guide to Monte Carlo Simulations in Statistical Physics* (Cambridge: Cambridge University Press)
[5] Alder B J and Wainwright T E 1957 *J. Chem. Phys.* **27** 1208
Alder B J and Wainwright T E 1959 *J. Chem. Phys.* **31** 459
[6] Rahman A 1964 *Phys. Rev.* **136** A405
Rahman A 1966 *J. Chem. Phys.* **45** 258
[7] Rapaport D C 1995 *The Art of Molecular Dynamics* (Cambridge: Cambridge University Press)
[8] Kremer K and Grest G S 1990 *J. Chem. Phys.* **92** 5057
[9] Binder K (ed) 1995 *Monte Carlo and Molecular Dynamics Simulations in Polymer Science* (New York: Oxford University Press)
[10] Metropolis N, Rosenbluth A W, Rosenbluth M N, Teller A N and Teller E 1953 *J. Chem. Phys.* **21** 1087
[11] Binder K (ed) 1979 *Monte Carlo Methods in Statistical Physics* (Berlin: Springer)
[12] Car R and Parrinello M 1985 *Phys. Rev. Lett.* **55** 2471
[13] Kohn W 1996 *Monte Carlo and Molecular Dynamics of Condensed Matter Systems* (Bologna: Societá Italiana di Fisica) p 561

Car R 1996 *Monte Carlo and Molecular Dynamics of Condensed Matter Systems* (Bologna: Societá Italiana di Fisica) p 601
[14] Berne B J and Thirumalai D 1986 *Annu. Rev. Phys. Chem.* **37** 401
Ceperley D M 1995 *Rev. Mod. Phys.* **67** 279
Ceperley D M 1996 *Monte Carlo and Molecular Dynamics of Condensed Matter Systems* (Bologna: Societá Italiana di Fisica) p 443
[15] Nielaba P 1997 *Annual Reviews of Computational Science* vol 5, ed D Stauffer (Singapore: World Scientific) p 137
Marx D and Müser M H 1999 *J. Phys.: Condens. Matter* **11** R117
[16] Tuckerman M E, Berne B J, Martyna G J and Klein M L 1993 *J. Chem. Phys.* **99** 2796
[17] Tuckerman M E and Hughes A 1998 *Classical and Quantum Dynamics in Condensed Phase Simulations* (Singapore: World Scientific)
[18] Müser M H 2001 *J. Chem. Phys.* **114** 6364
Schöffel P and Müser M H 2001 *Phys. Rev.* B **63** 224108
[19] Hansen J-P and McDonald I R 1986 *Theory of Simple Liquids* (San Diego, CA: Academic)
[20] Evans D J and Morris G P 1990 *Statistical Mechanics of Non-Equilibrium Liquids* (London: Academic)
Todd B D 2001 *Comput. Phys. Commun.* **142** 14
[21] Hess S, Kröger M, Lange W, Pereira Borgmeyer C, Schramek R, Voigt H and Weider T 1996 *Monte Carlo and Molecular Dynamics of Condensed Matter Systems* (Bologna: Societá Italiana di Fisica) p 823
Hess S and Evans D J 2001 *Phys. Rev.* E **64** 011207
Müller-Plathe F 1999 *Phys. Rev.* E **59** 4894
[22] Berthier L and Barrat J-L 2002 *J. Chem. Phys.* **116** 6228
[23] Binder K and Fratzl P 2001 *Phase Transformations in Materials* ed G Kostorz (Berlin: Wiley–VCH) p 409
[24] Chowdhury D, Santen L and Schadschneider A 2000 Statistical physics of vehicular traffic and some related systems *Phys. Rep.* **329** 119
Cetin N, Nagel K, Raney B and Voellmy A 2002 *Comput. Phys. Commun.* **147** 559
[25] Amaral L A N, Goldberger A L, Ivanov P C and Stanley H E 1998 *Phys. Rev. Lett.* **81** 2388
Amaral L A N, Goldberger A L, Ivanov P C and Stanley H E 1999 *Comput. Phys. Commun.* **121/122** 126
[26] Mantegna R N and Stanley H E 1999 *An Introduction to Econophysics: Correlations and Complexity in Finance* (Cambridge: Cambridge University Press)
[27] Herrmann H J, Hovi J P and Ludwig S (ed) 1998 *Physics of Dry Granular Media* (Dordrecht: Kluwer)
[28] Brandt A, Bernholc J and Binder K (ed) 2001 *Multiscale Computational Methods in Chemistry and Physics* (Amsterdam: IOS Press)
[29] Baschnagel J, Binder K, Doruker P, Gusev A A, Hahn O, Kremer K, Mattice W L, Müller-Plathe F, Murat M, Paul W, Santos S, Suter U W and Tries V 2000 Bridging the gap between atomistic and coarse-grained models of polymers: status and perspectives *Adv. Polym. Sci.* **152** 41
[30] Bates S and Wiltzius P 1989 *J. Chem. Phys.* **91** 3258
[31] Mainville J, Yang Y S, Elder K R, Sutton M, Ludwig K F Jr and Stephenson G B 1997 *Phys. Rev. Lett.* **78** 2787
[32] Marro J, Bortz A B, Kalos M H and Lebowitz J L 1975 *Phys. Rev.* B **12** 2000
Milchev A, Heermann D W and Binder K 1988 *Acta Metall.* **36** 377
[33] Sariban A and Binder K 1991 *Macromolecules* **24** 578
Reister E, Müller M and Binder K 2001 *Phys. Rev.* E **64** 041804
[34] Paul W, Smith G D, Yoon D Y, Farago B, Rathgeber S, Zirkel A, Willner L and Richter D 1998 *Phys. Rev. Lett.* **80** 2346
[35] Paul W 1997 *Computer Simulation Studies in Condensed Matter Physics* vol 11, ed D P Landau and H-B Schüttler (Berlin: Springer) p 197
[36] Rouse P E 1953 *J. Chem. Phys.* **21** 1273
[37] Doi M and Edwards S F 1986 *The Theory of Polymer Dynamics* (Oxford: Oxford University Press)
[38] Verlet L 1967 *Phys. Rev.* **159** 98
[39] Sprik M 1996 *Monte Carlo and Molecular Dynamics of Condensed Matter Systems* (Bologna: Societá Italiana di Fisica) p 43
[40] Andersen H C 1983 *J. Comput. Phys.* **52** 24
[41] Tuckerman M, Martyna G J and Berne B J 1992 *J. Chem. Phys.* **97** 1990
[42] Lebowitz J L, Percus J K and Verlet L 1967 *Phys. Rev.* **153** 250
[43] Nosé S 1984 *J. Chem. Phys.* **81** 511
[44] Hoover W G 1985 *Phys. Rev.* A **31** 1695
[45] Bennemann C, Paul W, Binder K and Dünweg B 1998 *Phys. Rev.* E **57** 843
[46] Andersen H C 1980 *J. Chem. Phys.* **72** 2384

[47] Frenkel D 1996 *Monte Carlo and Molecular Dynamics of Condensed Matter Systems* (Bologna: Societá Italiana di Fisica) p 3
[48] Kadanoff L P and Martin P C 1963 *Ann. Phys., NY* **24** 419
[49] Binder K 1979 *Monte Carlo Methods in Statistical Physics* ed K Binder (Berlin: Springer) p 1
[50] Horbach J and Kob W 1999 *Phys. Rev.* B **60** 3169
[51] Urbain G 1982 *Geochim. Cosmochim. Acta* **46** 1061
[52] Götze W and Sjögren L 1992 *Rep. Prog. Phys.* **55** 214
[53] van Beest B H W, Kramer G J and van Santen R A 1990 *Phys. Rev. Lett.* **64** 1955
[54] Vollmayr K, Kob W and Binder K 1996 *Phys. Rev.* B **54** 15808
[55] Price D L and Carpenter S M 1987 *J. Non-Cryst. Solids* **92** 153
[56] Mikkelsen J C 1984 *Appl. Phys. Lett.* **45** 1187
[57] Brébec G, Seguin R, Sella C, Bevenot J and Martin J C 1970 *Acta Metall.* **28** 327
[58] Scheidler P, Kob W, Latz A, Horbach J and Binder K 2001 *Phys. Rev.* B **67** 104204
[59] Horbach J, Kob W and Binder K 2001 *Eur. Phys. J.* B **19** 531
[60] Polian A, Vo-Tanh D and Richter P 2002 *Europhys. Lett.* **57** 375
[61] Todd B D 2001 *Comput. Phys. Commun.* **142** 14
[62] Varnik F and Binder K 2002 *J. Chem. Phys.* **117** 6336
[63] Horbach J and Binder K 2002 *J. Chem. Phys.* **117** 10796
[64] Müller-Plathe F 1997 *J. Chem. Phys.* **106** 6082
[65] Baschnagel J, Bennemann C, Paul W and Binder K 2000 *J. Phys.: Condens. Matter* **12** 6365
Binder K, Baschnagel J and Paul W 2002 *Prog. Polym. Sci.* **28** 115
[66] Landau L D and Lifshitz E M 1978 *Fluid Mechanics* (New York: Pergamon)
Barnes H A, Hutton J H and Walters K 1989 *Introduction to Rheology* (Amsterdam: Elsevier)
[67] Todd B D and Evans D J 1997 *Phys. Rev.* E **55** 2800
[68] Green M S 1954 *J. Chem. Phys.* **22** 398
Kubo R 1957 *J. Phys. Soc. Japan* **12** 570